

# The Influence of n-AlGaN Inserted Layer on the Performance of Back-Illuminated AlGaN-Based p-i-n Ultraviolet Photodetectors

Yiren Chen, Zhiwei Zhang, Zhiming Li, Hong Jiang, Guoqing Miao, and Hang Song\*

In this paper, comparison between back-illuminated p-i-n AlGaN-based ultraviolet photodetectors (UV-PDs) with and without an n-AlGaN inserted layer is carried out. The results show that the introduction of n-AlGaN interlayer significantly reduces the dark current of AlGaN-based UV-PDs. The mechanism involved is clarified and can be attributed to the role of n-AlGaN interlayer which depletes to isolate the leakage paths generated by dislocations of AlGaN material. Besides, it also greatly improves the spectral performances of the p-i-n AlGaN-based UV-PDs, which can be related to the additional built-in electric fields introduced by n-AlGaN inserted layer that contribute to separate and transport the photon-generated carriers.

## 1. Introduction

As the third generation of semiconductor, GaN-based materials have achieved a great success in the fields of optoelectronics and microelectronics, such as light emitting diodes (LEDs),<sup>[1]</sup> laser diodes (LDs),<sup>[2]</sup> high-voltage and high-frequency power devices,<sup>[3,4]</sup> and so on. Recently, there is a growing concern over the ultraviolet photodetectors (UV-PDs) based on AlGaN ternary alloy material, because of its wide direct band gap, full solid-state, intrinsic cut-off that makes it filter-free, and the potential applications in flame/engine monitoring and detection, ozone layer monitoring, missile warning and guidance, free-space optical communication, and chemical/biological agent sensing.<sup>[5]</sup> The development of AlGaN-based UV-PDs will provide a promising alternative instead of the traditional photomultiplier tube (PMT) or silicon-based photodiode with a complex and costly ultraviolet band-pass filter.<sup>[6]</sup>

So far, many different types of AlGaN-based UV-PDs have been proposed, including photoconductors, p-n and p-i-n photodiodes, metal-semiconductor-metal (MSM) detectors and Schottky barrier photodiodes.<sup>[7]</sup> The back-illuminated p-i-n structure is considered to be the most suitable one for hybrid integration with silicon CMOS read-out integrated circuit

(ROIC) chip by indium bump technology and realize focal plane array (FPA) for UV imaging.<sup>[8]</sup> However, the performance of back-illuminated p-i-n AlGaN-based UV-PDs is hindered due to high density dislocation (over  $10^9 \text{ cm}^{-2}$ ) in AlGaN material grown by mainstream heteroepitaxy,<sup>[9]</sup> which has been proved to be the main leakage current channels for nitride semiconductor devices under reverse bias.<sup>[10]</sup> Thus, the high density dislocation in AlGaN material results in high dark current, which deteriorates the photoelectric response characteristic of devices simultaneously. To suppress the influence of dislocations on reverse-bias leakage, many investigations have been carried out. Kumar et al.<sup>[11]</sup> have demonstrated

improved device performance of GaN-based UV-PDs by inserting ultrathin HfO<sub>2</sub> layer, which significantly reduced the dark current of the PDs and obtained excellent photoresponsivity. Sun et al.<sup>[12]</sup> have introduced SiO<sub>2</sub> nanoparticles (SNPs) on the surface of GaN-based photodetector to passivate its dislocations so as to suppress the dark current and improve responsivity. Le et al.<sup>[13]</sup> have proposed a thin undoped InGaN interlayer prior to electron blocking layer (EBL) to further suppressed the electron leakage and thus improved the characteristics of InGaN-based blue-violet LDs. Zang et al.<sup>[14]</sup> have significantly suppressed the dark current of Ge PD by introducing the metal-interlayer-semiconductor-metal (MISM) structure with a TiO<sub>2</sub> interlayer.

In this letter, a thin homogeneous n-AlGaN inserted layer is introduced into the light absorption layer of back-illuminated p-i-n AlGaN-based UV-PD, the influence of which on the performance of the UV-PD is also investigated. A more complete understanding the role of the n-AlGaN interlayer will be beneficial to optimize the design of the back-illuminated p-i-n AlGaN-based UV-PD.

## 2. Experimental Section

In order to evaluate the role of the n-AlGaN inserted layer in detail, we vary its thickness for different samples. **Figure 1(a)** shows the schematic structures of the back-illuminated p-i-n AlGaN-based UV-PDs with thickness of n-AlGaN inserted layers 0 nm, 20 nm, and 60 nm, corresponding to sample A, B, and C,

Dr. Y. Chen, Dr. Z. Zhang, Prof. Z. Li, Prof. H. Jiang,  
Prof. G. Miao, Prof. H. Song  
State Key Laboratory of Luminescence and Applications  
Changchun Institute of Optics, Fine Mechanics and Physics  
Chinese Academy of Sciences  
3888 Dongnanhu Road, Changchun 130033, China  
E-mail: songh@ciomp.ac.cn

DOI: 10.1002/pssa.201700358

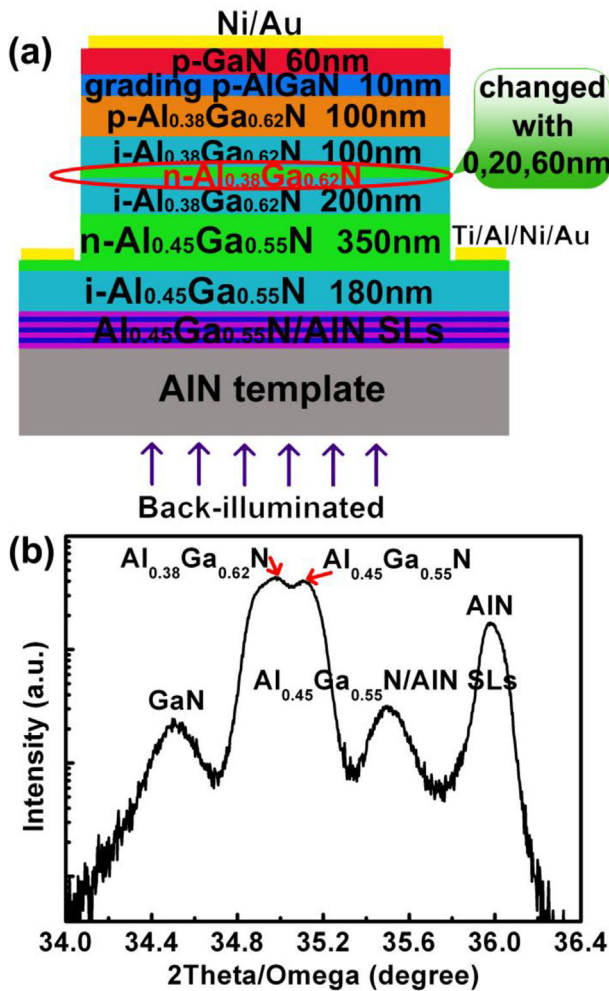


**Figure 1.** Device structure and material characterization. a) Cross-section of the back-illuminated p-i-n AlGaN-based photodetectors with different thickness of n-AlGaN inserted layers, (b) the typical (0002) plane  $2\theta$ - $\omega$  scan curve for wafers by HRXRD.

respectively. All of them were grown on 2 in. c-plane single-polished sapphire substrate by low-pressure metal-organic chemical vapor deposition (MOCVD). In the process, trimethylgallium (TMGa), trimethylaluminum (TMAI), and ammonia ( $\text{NH}_3$ ) were, respectively, used as Ga, Al, and N precursors while dicyclopentadienyl magnesium ( $\text{Cp}_2\text{Mg}$ ) and silane ( $\text{SiH}_4$ ) as the p- and n-type dopants. Prior to the growth, the sapphire substrate was thermally desorbed under  $\text{H}_2$  ambient at  $1050^\circ\text{C}$  for 10 min. Following the AlN buffer layer grown by normal two-step method,<sup>[15]</sup> ten periods  $\text{Al}_{0.45}\text{Ga}_{0.55}\text{N}/\text{AlN}$  (6 nm/6 nm) superlattices (SLs) were grown to suppress the dislocation extension from AlN template and regulate the stress so as to avoid the formation of cracks.<sup>[16]</sup> Then, a 180-nm-thick  $\text{i-Al}_{0.45}\text{Ga}_{0.55}\text{N}$  layer and a 350-nm-thick  $\text{n-Al}_{0.45}\text{Ga}_{0.55}\text{N}$  layer were grown on SLs in succession. Subsequently, distinguished from the conventional p-i-n structure (sample A), a 20-nm-thick and a 60-nm-thick  $\text{n-Al}_{0.38}\text{Ga}_{0.62}\text{N}$  layer was inserted in the 300-nm-thick  $\text{i-Al}_{0.38}\text{Ga}_{0.62}\text{N}$  of samples B and C during the

growth process, respectively. After finishing the deposition of 100-nm-thick  $\text{p-Al}_{0.38}\text{Ga}_{0.62}\text{N}$  layer, a thin p-AlGaN layer ( $\approx 10$  nm) with Al component gradient was grown as a transition layer. Finally, a p-GaN layer was grown on top of the p-AlGaN graded component layer to reduce the contact resistance of p-type electrode. The carrier concentration of  $\text{n-Al}_{0.45}\text{Ga}_{0.55}\text{N}$ ,  $\text{n-Al}_{0.38}\text{Ga}_{0.62}\text{N}$ ,  $\text{p-Al}_{0.38}\text{Ga}_{0.62}\text{N}$  and p-GaN layers are  $1 \times 10^{18}$ ,  $5 \times 10^{17}$ ,  $2 \times 10^{17}$ , and  $6 \times 10^{17} \text{ cm}^{-3}$ , respectively, which were measured based on the epitaxial wafer by electrochemical capacitance–voltage (ECV) method. Figure 1(b) shows the typical (0002) plane  $2\theta$ - $\omega$  scan curve for three epitaxial wafers by high resolution X-ray diffraction (HRXRD). As can be seen, there are five peaks located at  $34.507$ ,  $35$ ,  $35.15$ ,  $35.5$ , and  $36^\circ$ , corresponding to GaN,  $\text{Al}_{0.38}\text{Ga}_{0.62}\text{N}$ ,  $\text{Al}_{0.45}\text{Ga}_{0.55}\text{N}$ ,  $\text{Al}_{0.45}\text{Ga}_{0.55}\text{N}/\text{AlN}$  SLs, and AlN layers, respectively.

After finishing the epitaxial growth, the wafers were rapidly annealed at  $800^\circ\text{C}$  under the  $\text{N}_2$  atmosphere to activate the Mg dopants in the p-type AlGaN and GaN layers. In the subsequent process of device fabrication, inductively-coupled plasma (ICP) dry etching method was adopted to etch the material to the  $\text{n-Al}_{0.45}\text{Ga}_{0.55}\text{N}$  layer, leaving a  $500\text{-}\mu\text{m}$ -diameter mesa. Surrounding the mesa, a Ti/Al/Ni/Au (30/100/150/200 nm) ring electrode was deposited onto the  $\text{n-Al}_{0.45}\text{Ga}_{0.55}\text{N}$  using electron-beam evaporation. Similarly, on top of the p-GaN mesa, a Ni/Au (150/200 nm) circle electrode was fabricated. The whole device was then annealed at  $700^\circ\text{C}$  for 60 s in  $\text{N}_2$  atmosphere to realize ohmic contact electrodes.

### 3. Results and Discussion

To understand the strain state in the layers, asymmetrical reciprocal space mapping (RSM) is measured around  $(\bar{1}0\bar{1}5)$  reflection. Figure 2 show the RSM of sample B (with n-AlGaN interlayer) as a representative. It should be noted that the  $\text{n-Al}_{0.38}\text{Ga}_{0.62}\text{N}$  interlayer has the same Al content as the  $\text{i-Al}_{0.38}\text{Ga}_{0.62}\text{N}$  layer, the RSMs of the three samples are basically the same, so we use the RSM of samples B on behalf. Each reciprocal lattice point (RLP) shown in the RSM represents each individual layer. The RLPs mainly correspond to the AlN buffer layer, the AlGaN/AlN superlattices (SLs), the  $\text{Al}_{0.45}\text{Ga}_{0.55}\text{N}$  layer and the  $\text{Al}_{0.38}\text{Ga}_{0.62}\text{N}$  layer, which are consistent with the material structure except that the thin GaN layer is beyond the scan range. In Figure 2,  $q_x$  and  $q_z$  are on behalf of the directions parallel and perpendicular to the interface of epilayer and substrate, which can be used to calculate the in-of-plane lattice constant through  $a = (4(h^2 + hk + k^2)/3q_x^2)^{1/2}$  and out-of-plane lattice constant through  $c = l/q_z$ , respectively.<sup>[17,18]</sup> Here,  $h$ ,  $k$ , and  $l$  are Miller indices. The lattice constants for relaxed AlN and GaN are ( $a = 0.31127$  nm,  $c = 0.49817$  nm) and ( $a = 0.31891$  nm,  $c = 0.51855$  nm), respectively. Therefore, the RLPs denoted as ( $q_x$ ,  $q_z$ ) for the relaxed AlN and GaN can be calculated as  $(-3.71, 10.037)$  and  $(-3.62, 9.642)$  for  $(\bar{1}0\bar{1}5)$  reflection, respectively. The connection line between the RLPs of the relaxed AlN and GaN will represent fully relaxed  $\text{Al}_x\text{Ga}_{1-x}\text{N}$  while the connection line between the RLPs of the relaxed AlN and GaN strained to AlN will represent  $\text{Al}_x\text{Ga}_{1-x}\text{N}$  fully strained to AlN, as shown in Figure 2. It should be noted that the points of relaxed GaN and GaN strained to AlN are beyond the coordinates in Figure 2. It

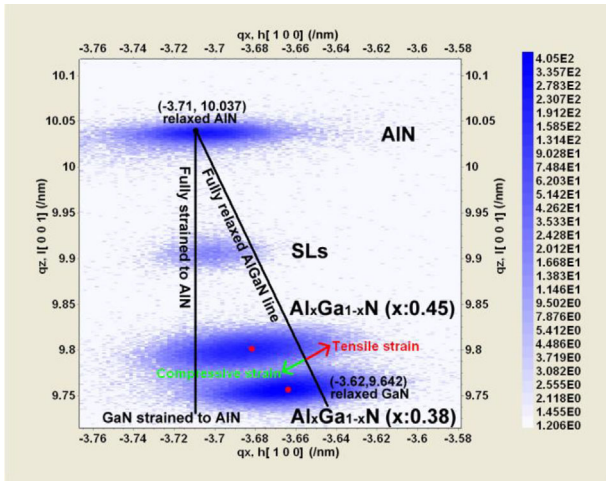


**Figure 2.** The asymmetrical reciprocal space map around  $(10\bar{1})$  reflection of samples B as a representative.

has been concluded that the region (indicated by green arrow) to the left of relaxation line represents  $\text{Al}_x\text{Ga}_{1-x}\text{N}$  under compressive strain, while the region (indicated by red arrow) to the right of relaxation line represents  $\text{Al}_x\text{Ga}_{1-x}\text{N}$  under tensile strain.<sup>[18]</sup> As can be seen in Figure 2, the RLPs of the  $\text{Al}_{0.45}\text{Ga}_{0.55}\text{N}$  layer and the  $\text{Al}_{0.38}\text{Ga}_{0.62}\text{N}$  layer (red points) locate at the left side of the fully relaxed line which means that both present compressive strain.

An Agilent B1500A semiconductor parameter analyzer is employed to measure the current–voltage ( $I$ – $V$ ) characteristic of the devices. **Figure 3** shows the dark current of the three back-illuminated p-i-n AlGaIn-based UV-PD samples A, B, and C in semi-logarithmic coordinate. As can be seen, the dark current of the three samples at reverse bias follows a sequence of  $A > B > C$ , which means that the dark current decreases with the increase of the thickness of the n-AlGaIn inserted layer. The dark current of sample C is about 5 nA at  $-10$  V bias, which is significantly reduce by more than four orders of magnitude compared to that of sample A (about 33  $\mu\text{A}$  at  $-10$  V bias). In

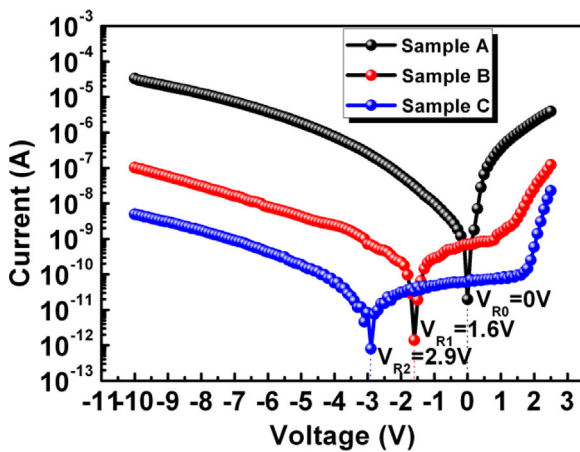


**Figure 3.** The dark currents of back-illuminated p-i-n AlGaIn-based UV-PDs using semi-logarithmic coordinate.

addition, the samples with n-AlGaIn inserted layer present a zero offset in  $I$ – $V$  characteristic, and the offset voltage value is increased as the thickness of the n-AlGaIn inserted layer increases. In this work, the offset voltage values for samples B and C are about  $-1.6$  and  $-2.9$  V, respectively, labbed as  $V_{R1} = 1.6$  V and  $V_{R2} = 2.9$  V, corresponding to the  $V_{R0} = 0$  V for sample A, as shown in Figure 3.

To clarify this phenomenon, the related space charge profiles and energy band diagrams under reverse bias for p-i-n structure with/without n-AlGaIn inserted layer are illustrated in **Figure 4** (a)–(d). As seen in Figure 4(a), at the interfaces of p-AlGaIn/i-AlGaIn and i-AlGaIn/n-AlGaIn in conventional p-i-n structure (sample A), the space charge regions will be formed by the carrier diffusion due to carrier concentration gradient and result in the formation of built-in electric fields  $E_{pi}$  and  $E_{ni}$ , which will be enlarged with the increase of applied reverse voltage  $E_{appl}$ . Simultaneously, the energy band of sample A (Figure 4(c)) will further tilt along with the increase of  $E_{appl}$ , and the depletion regions at the interfaces of p-AlGaIn/i-AlGaIn and i-AlGaIn/n-AlGaIn also expand on both sides. However, as for p-i-n structure with n-AlGaIn inserted layer (seen in Figure 4(b)), in addition to the process mentioned above, there are two additional interfaces located at both sides of  $n_1$ -AlGaIn interlayer. The space charge regions formed at the interfaces of  $i_1$ -AlGaIn/ $n_1$ -AlGaIn and  $n_1$ -AlGaIn/ $i_2$ -AlGaIn will generate opposite direction built-in electric fields  $E_{ni1}$  and  $E_{ni2}$ . With the increase of  $E_{appl}$ , the  $E_{ni2}$  is suppressed while the  $E_{ni1}$  is enhanced. Meanwhile, the main depletion region in the n-AlGaIn inserted layer is gradually enlarging along the direction signed in Figure 4(d). Using  $V_B$  as the critical point where the n-AlGaIn inserted layer is depleted under certain initial reverse bias, the dark current reaches its minimum at  $V_B$ . For sample A, the  $V_B$  overlaps with zero bias point ( $V_{R0}$ ) without any offset happens. Unlike sample A, the  $V_B$  values of samples B and C are offset because of the presence of the n-AlGaIn interlayer, corresponding to  $V_{R1}$  and  $V_{R2}$ ,

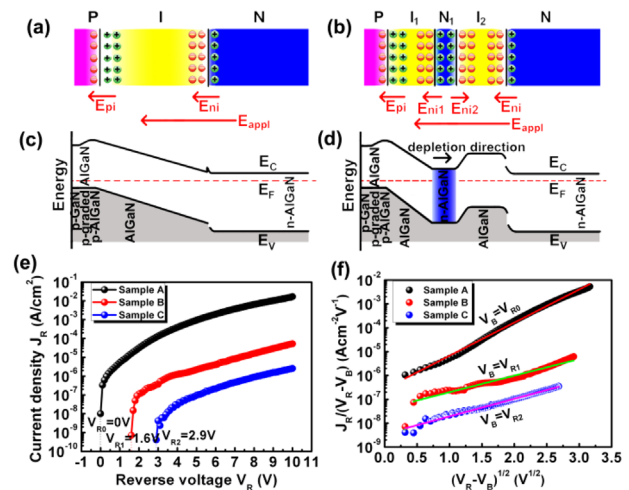


**Figure 4.** Space charge profiles for p-i-n AlGaIn-based UV-PDs (a) without n-AlGaIn inserted layer, (b) with n-AlGaIn inserted layer. c) and d) Energy band diagram for (a) and (b), respectively. e) The dark current density curves of samples A–C under the reverse bias. f) Linear relationship between  $\log(J_R/(V_R - V_B))$  and  $(V_R - V_B)^{1/2}$  for three samples.

respectively. The value of  $V_B$  is directly related to the thickness of the n-AlGa<sub>N</sub> inserted layer, the thicker the n-AlGa<sub>N</sub> is, the greater additional electric field to form the depletion region is needed. Therefore, it is reasonable for the result that  $V_{R1}$  is less than  $V_{R2}$  while the n-AlGa<sub>N</sub> inserted layer of sample C is thicker than that of sample B.

Under the reverse bias, the dark current of samples A, B, and C are presented in Figure 4(e). Based on Frenkel-Poole emission, the current density is given by<sup>[19]</sup>

$$J \propto E_{\text{exp}} \left[ -\frac{q \left( \Phi_B - \sqrt{\frac{qE}{\pi\epsilon}} \right)}{k_B T} \right] \quad (1)$$

where  $E$  is the applied electric field,  $q$  is the elementary charge,  $\Phi_B$  is the voltage barrier in zero applied electric field,  $k_B$  is the Boltzmann's constant, and  $T$  is the absolute temperature. Assuming a linear dependence of  $E$  with reverse voltage ( $V_R$ ), and taking the critical voltage  $V_B$  for the depletion of n-AlGa<sub>N</sub> inserted layer into account, Eq. (1) can be transformed into the following Eq. (2)

$$\log \left( \frac{J_R}{V_R - V_B} \right) \propto (V_R - V_B)^{\frac{1}{2}} \quad (2)$$

Taken the logarithm of reverse current density ( $J_R$ ) divided by  $(V_R - V_B)$ , it shall be a linear relationship with  $(V_R - V_B)^{1/2}$ . Figure 4(f) shows  $\log(J_R/(V_R - V_B))$  as a function of  $(V_R - V_B)^{1/2}$ , which follows the expected evolution predicted by Eq. (2). This confirms that the main dark current in p-i-n AlGa<sub>N</sub>-based PDs with/without the n-AlGa<sub>N</sub> interlayer obeys the Frenkel-Poole emission model, although the existing of diffusion current and drift current. The dark current associated with the Frenkel-Poole emission has been proved to be the carrier transportation via conductive dislocations of nitride semiconductor materials under reverse bias.<sup>[20]</sup> Therefore, the mechanism of suppressing the dark current of the p-i-n AlGa<sub>N</sub>-based UV-PD with n-AlGa<sub>N</sub> inserted layer can be ascribed to the isolation effect of the depletion layer on the leakage channels formed by conductive dislocations.

The spectral responsivity and the corresponding external quantum efficiency (EQE) at zero-bias for three samples are measured using a xenon lamp as light source, a chopper, a monochromator, a lock-in amplifier, and a calibrated UV-enhanced silicon photodetector as standard reference. The spectral response range is measured from 260 to 380 nm, and the monochromatic light irradiates from the sapphire substrate side of the samples to realize back-illumination. As can be seen in **Figure 5**, the peak responsivity of sample A at zero bias locates at 289 nm with a value of  $77 \text{ mA W}^{-1}$  and the corresponding EQE only reaches up to 33.2%. In contrast, samples B and C have a peak responsivity of 140 and  $157 \text{ mA W}^{-1}$  at 290 nm, corresponding to an EQE of 60.1 and 67.4%, respectively. The slight difference of peak wavelength can be ascribed to the tiny fluctuation of Al component in AlGa<sub>N</sub> material. Obviously, the spectral performance of the p-i-n AlGa<sub>N</sub>-based UV-PDs with n-AlGa<sub>N</sub> interlayer has been greatly improved at zero-bias. It can

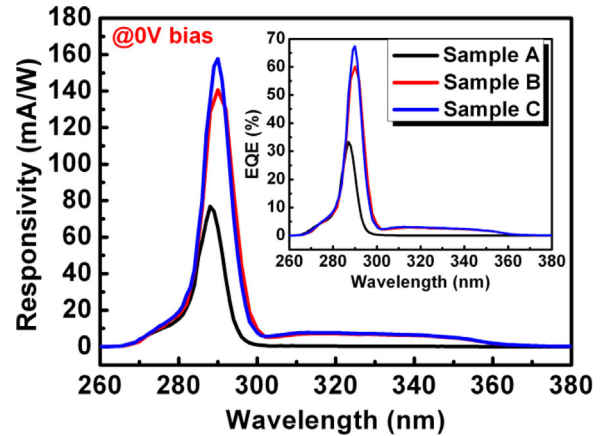


**Figure 5.** The comparison of spectral responsivities under zero-bias. The inset shows the corresponding EQE.

be attributed to the additional built-in electric fields induced by n-AlGa<sub>N</sub> interlayer, which contribute to separate and transport the photon-generated carriers. With the addition of n-AlGa<sub>N</sub> interlayer thickness, the spectral performance will be further improved (e.g., sample C). However, as the thickness increases to a certain extent, the further enhancement of spectral performance will be suppressed due to the increase of recombination probability in a wide light absorption layer. In our experiments, when the total thickness of i-AlGa<sub>N</sub> light absorption layer is fixed at 300 nm, the spectral responsivity is close to the saturation value when the thickness of n-AlGa<sub>N</sub> interlayer is around 60 nm.

In conclusion, we demonstrate the influence of n-AlGa<sub>N</sub> inserted layer on the performance of back-illuminated p-i-n AlGa<sub>N</sub>-based UV-PDs. The results show that the introduction of n-AlGa<sub>N</sub> inserted layer significantly reduces the dark current by more than four orders of magnitude and greatly improves its responsivity and EQE at zero bias. The mechanism involved can be attributed to the role of interlayer which depletes to isolate the leakage current channels generated by dislocations of AlGa<sub>N</sub> material. In addition, the improvement of spectral performance directly relates to the additional built-in electric fields induced by n-AlGa<sub>N</sub> inserted layer.

## Acknowledgments

This work was partially supported by National Natural Science Foundation of China (NSFC) (Grant Nos. 61504144, 51472230), the Jilin Provincial Science and Technology Department (Grant No. 20170520156JH).

## Conflict of Interest

The authors declare no conflict of interest.

## Keywords

AlGa<sub>N</sub>, inserted layers, p-i-n structures, ultraviolet photodetectors

Received: June 9, 2017

Revised: October 8, 2017

Published online: December 6, 2017

- 
- [1] Y. Liao, C. Thomidis, C. Kao, A. Moldawer, W. Zhang, Y. Chang, A. Yu. Nikiforov, E. Bellotti, T. D. Moustakas, *Phys. Status Solidi RRL* **2010**, 4, 49.
- [2] D. Kasahara, D. Morita, T. Kosugi, K. Nakagawa, J. Kawamata, Y. Higuchi, H. Matsumura, T. Mukai, *Appl. Phys. Express* **2011**, 4, 072103.
- [3] J. W. Chung, W. E. Hoke, E. M. Chumbes, T. Palacios, *IEEE Electron Dev. Lett.* **2010**, 31, 195.
- [4] Y. Cordier, *Phys. Status Solidi A* **2015**, 212, 1049.
- [5] T. Tut, T. Yelboga, E. Ulker, E. Ozbay, *Appl. Phys. Lett.* **2008**, 92, 103502.
- [6] E. Cicek, R. McClintock, Z. Vashaei, Y. Zhang, S. Gautier, C. Y. Cho, M. Razeghi, *Appl. Phys. Lett.* **2013**, 102, 051102.
- [7] M. B. Reine, A. Hairston, P. Lamarre, K. K. Wong, S. P. Tobin, A. K. Sood, C. Cooke, M. Pophristic, S. Guo, B. Peres, R. Singh, C. R. Eddy, U. Chowdhury, M. M. Wong, R. D. Dupuis, T. Li, S. P. DenBaars, *Proc. SPIE* **2006**, 6119, 611901.
- [8] E. Cicek, Z. Vashaei, E. K. Huang, R. McClintock, M. Razeghi, *Opt. Lett.* **2012**, 37, 896.
- [9] S. W. Kaun, M. H. Wong, S. Dasgupta, S. Choi, R. Chung, U. K. Mishra, J. S. Speck, *Appl. Phys. Express* **2011**, 4, 024101.
- [10] W. P. Hsu, M. J. Manfra, R. J. Molnar, B. Heying, J. S. Speck, *Appl. Phys. Lett.* **2002**, 81, 79.
- [11] M. Kumar, B. Tekcan, A. K. Okyay, *J. Vac. Sci. Technol. A* **2015**, 33, 021204.
- [12] X. Sun, D. Li, H. Jiang, Z. Li, H. Song, Y. Chen, G. Miao, *Appl. Phys. Lett.* **2011**, 98, 121117.
- [13] L. C. Le, D. G. Zhao, D. S. Jiang, P. Chen, Z. S. Liu, J. Yang, X. G. He, X. J. Li, J. P. Liu, J. J. Zhu, S. M. Zhang, H. Yang, *Opt. Express* **2014**, 22, 11392.
- [14] H.-J. Zang, G.-S. Kim, G.-J. Park, Y.-S. Choi, H.-Y. Yu, *Opt. Lett.* **2016**, 41, 3686.
- [15] Y. Chen, H. Song, D. Li, X. Sun, H. Jiang, Z. Li, G. Miao, Z. Zhang, Y. Zhou, *Mater. Lett.* **2014**, 114, 26.
- [16] E. Cicek, R. McClintock, C. Y. Cho, B. Rahnama, M. Razeghi, *Appl. Phys. Lett.* **2013**, 103, 181113.
- [17] Y. P. Gong, K. Xing, T. Wang, *Appl. Phys. Lett.* **2011**, 99, 171912.
- [18] A. Kadir, C. C. Huang, K. E. K. Lee, E. A. Fitzgerald, S. J. Chua, *Appl. Phys. Lett.* **2014**, 105, 232113.
- [19] E. Arslan, S. Buttun, E. Ozbay, *Appl. Phys. Lett.* **2009**, 94, 142106.
- [20] P. Kozodoy, J. P. Ibbetson, H. Marchand, P. T. Fini, S. Keller, J. S. Speck, S. P. DenBaars, U. K. Mishra, *Appl. Phys. Lett.* **1998**, 73, 975.